Ability of monocentric close-coupling expansions to describe ionization in atomic collisions

B. Pons
Centre Lasers Intenses et Applications, UMR 5107 du CNRS, Université de Bordeaux-I, 351 Cours de la Libération, F-33405 Talence, France
(Received 28 July 2000; published 6 December 2000)

We elicit the ability of monocentric close-coupling expansions to describe ionization in $\bar{p}+\mathrm{H}(1s)$ collisions. We show that expansions in terms of exponentially decaying basis functions are definitively unable to provide reliable ionizing distributions in the outgoing part of the collision, since they cannot be enlarged enough to suitably reproduce the outer part of the continuum wave functions. We review the construction of a monocentric expansion in terms of spherical Bessel functions confined in a box that has recently been proposed to better describe the ionizing wave functions and hence overcome the failure of the usual expansions [B. Pons, Phys. Rev. Lett. **84**, 4569 (2000)]. We ascertain the reliability of the method and enlarge our previous study of ionizing $\bar{p}+\mathrm{H}(1s)$ collisions from low to high impact velocities.

DOI: 10.1103/PhysRevA.63.012704 PACS number(s): 34.10.+x, 34.50.Fa, 36.10.−k

I. INTRODUCTION

Ionization in ion-atom collisions is quite an old topic whose revival is partly due to the recent advent of recoil ion momentum spectroscopy [2]. Combined recoil-ion–electron spectroscopy yields a complete momentum determination of all outgoing particles in single-ionization collisions [3]. The previously standard electron momentum spectroscopy provided angular and energy distributions of the ejected electrons [4], of great help in probing the reliability of (mainly) perturbative and classical descriptions of ionization [5]. Despite fair advances over the last 20 years, it still remains difficult to describe even the main feature of the ionization mechanism. An in-depth understanding of the dynamics requires the time evolution of the ejected electron distributions along the collision and theoretical descriptions are expected to complement experiments in that way.

So in their classical trajectory Monte Carlo (CTMC) study of the ionization mechanism in ion-atom collisions, Illescas and Riera [6] recently stressed that, even at low velocities, ionization takes place within a small range $0<t<10$ a.u.; later on, the so-called postcollision interaction (PCI, [7]) effects are found to be secondary and the electrons move quasifreely. This scenario has to be verified by a time-dependent quantum description of the process. One can naturally invoke the close-coupling method, which is based on expanding the total electronic wave function over a finite set of basis functions spanning the main reaction channels, since it provides accurate total ionization cross sections (see, for instance, [8]). Nevertheless, a large-scale monocentric expansion, in terms of Slater-type orbitals (STOs), has recently been shown to yield unphysical ionizing distributions in the outgoing part of $\bar{p}+\mathrm{H}(1s)$ collisions [1]. A monocentric close-coupling expansion in terms of spherical Bessel functions confined in a finite box has thus been proposed to better describe the ionizing continuum wave functions [1]. Its implementation in low velocity $\bar{p}+\mathrm{H}(1s)$ collisions led to a reliable picture of the ionization mechanism that essentially confirmed the CTMC description of Illescas and Riera.

In the present contribution, we aim at clarifying how far the ''usual'' expansions, such as the STO one, can accurately describe ionization. Illustrations are given for monocentric calculations in $\bar{p}+\mathrm{H}(1s)$ collisions. Such collisions do not support charge exchange reaction paths; further, the electron capture to the continuum (ECC) [7,9] and saddle-point [7,10] ionization mechanisms, which are specific features of positively charged ion impact, cannot contributed therein to electron ejection. $\bar{p}+\mathrm{H}(1s)$ collisions thus provide the fundamental testing ground to elicit the ability of close-coupling expansions to describe ionization accurately. We will discuss how our conclusions, drawn from monocentric STO calculations, hold for other expansions using the same kind of underlying basis function [8,11–17].

The paper is organized as follows. Section II A outlines the monocentric close-coupling formalism; the STO and spherical Bessel expansions are described in Sec. II B. Both expansions are shown to provide accurate probabilities and total cross sections for ionization and excitation in Sec. III A; in Sec. III B, ejected electron distributions are compared and mark out the limitations of the usual (STO) expansions; further, the behavior of the Bessel ionizing distributions is analyzed as a function of the impact velocity; afterwards, we ascertain the reliability of these distributions and finally expose the origin of the failure of the usual expansions.

Atomic units are used throughout unless otherwise stated.

II. THE MONOCENTRIC CLOSE-COUPLING FRAMEWORK

A. General formalism

Within the impact parameter approach, the projectile follows classical rectilinear trajectories with constant velocity **v** and impact parameter **b**. Monocentric close-coupling expansions for a single electron total wave function read

$$\Psi(\mathbf{r},v,b,t)=\sum_{E_nlm} a_{E_nlm}(v,b,t)\,\phi_{E_nlm}(\mathbf{r})e^{-iE_nt}, \qquad (1)$$

where $\phi_{E_nlm}(\mathbf{r})$ are atomic eigenstates mostly obtained by diagonalization of the target Hamiltonian H_0 in a basis of

target-centered orbitals, and $E_n=\langle\phi_{E_nlm}|H_0|\phi_{E_nlm}\rangle$. The diagonalization procedure also yields (L^2 square integrable) wave functions of positive energy, usually called pseudostates, so that Ψ spans both excitation ($E_n<0$) and ionization ($E_n>0$) channels. The amplitudes $a_{E_nlm}(v,b,t)$ are numerically obtained by solving the usual set of differential coupled equations that results from the insertion of the ansatz (1) in the eikonal equation,

$$\left(H_0+V_b-i\frac{d}{dt}\right)\Psi=0, \tag{2}$$

where $V_b=-Q_P/|\mathbf{r}-\mathbf{R}(t)|$ is the electron-projectile interaction, with Q_P the projectile charge and $\mathbf{R}(t)=\mathbf{b}+\mathbf{v}t$ the internuclear vector. The coupled equation set is integrated from $t_{ini}=-50/v$ a.u., where $a_{E_nlm}(v,b,t_{ini})=\delta_{E_nlm,-0.5\,0\,0}$ for the H($1s$) initial state, up to $t_{max}=500/v$ a.u., yielding the inelastic transition probabilities $P_{E_nlm}(v,b)=|a_{E_nlm}(v,b,t_{max})|^2$ and corresponding cross sections $\sigma_{E_nlm}(v)=\int bP_{E_nlm}(v,b)db$.

Our basic tool to illustrate the ionization dynamics will be the time evolution of the ionizing density. A clear picture further requires a simultaneous display of the density in configuration and momentum spaces. The ionizing part Ψ_{ion} of the total wave function is extracted from Eq. (1) under the restriction $E_n>0$. Such a condition does not provide a separation of the capture and ionization fluxes; nevertheless, we focus in the present work on $\bar{p}+$H($1s$) collisions in which the former process does not exist. For positively charged ion impact, the ionization channel should be represented by the states that are unbound with respect to both the target and the moving projectile [18]. In the laboratory-fixed reference frame, $\mathbf{r}=(x,y,z)$ with $\hat{\mathbf{x}}=\hat{\mathbf{b}}$, $\hat{\mathbf{z}}=\hat{\mathbf{v}}$, and $\hat{\mathbf{y}}$ perpendicular to the collisional plane. We obtain the two-dimensional electron distribution in coordinate space, integrating over y,

$$\rho_{ion}(x,z,v,b,Z)=\int|\Psi_{ion}(\mathbf{r},v,b,t)|^2dy \tag{3}$$

as a function of the scaled time $Z=vt$. The wave function in momentum space is numerically obtained by fast Fourier transform [19] of Ψ_{ion}, leading to the two-dimensional electron distribution in momentum space:

$$\tilde{\rho}_{ion}(p_x,p_z,v,b,Z)=\int|\tilde{\Psi}_{ion}(\mathbf{p},v,b,t)|^2dp_y, \tag{4}$$

where p_x and p_z are the so-called transverse and longitudinal electronic momenta.

B. Basis expansions

The monocentric expansions mainly differ in the underlying basis used to construct the atomic eigenstates $\phi_{E_nlm}(\mathbf{r})$. Hereinafter, these are first obtained as linear combinations of even-tempered STOs that diagonalize the Hamiltonian:

$$\phi_{E_nlm}(\mathbf{r})=\sum_j c_j^{nl}e^{-\alpha_jr}r^l\mathcal{Y}_l^m(\hat{\mathbf{r}}) \tag{5}$$

with $\mathcal{Y}_l^m(\hat{\mathbf{r}})=Y_l^m(\hat{\mathbf{r}})$ if $m=0$, and $\mathcal{Y}_l^m(\hat{\mathbf{r}})=Y_l^m(\hat{\mathbf{r}})\pm(-1)^mY_l^{-m}(\hat{\mathbf{r}})$ otherwise. The parameters α_j are in geometrical series which can be different for each l symmetry: $\alpha_j=\alpha_0\beta^j$ with $0\leqslant j\leqslant j_{max}$. The STO basis is thus defined by l_{max}, the maximum angular momentum introduced, and by the geometrical sets $\{\alpha_0,\beta,j_{max}\}_{l=0,\ldots,l_{max}}$ (all spherical harmonics are usually included up to $m=l$). Bound and unbound eigenstates can be exactly described in the limit of a complete set covering the entire space. In practice, the underlying basis is truncated and this mainly affects the description of the atomic continuum which thus consists of a few pseudostates that are exponentially spaced in energy scale. Further, the truncated expansion (5) generally prevents the pseudostates from fulfilling the correct asymptotic behavior $\sin(pr-l\pi/2)/pr$. Gaussian, (scaled) hydrogenic, and Sturmian orbitals are also currently used in the usual close-coupling calculations [8,11–17]. All of them exponentially decay with r and are able to span a similar configuration space, provided the (limited) sequence of orbital exponents is suitably chosen. Moreover, all these sets lead in practice to equivalent descriptions of the continuum [8,11–15]; a large-scale STO set is therefore representative of all monocentric expansions in terms of exponentially decaying basis functions.

Recently, a monocentric expansion in terms of spherical Bessel functions confined in a finite box was proposed to better describe the ionizing continuum wave functions [1]. The configuration space is reduced to a spherical box of radius r_{max} centered on the target. Further, it is assumed that the electron cannot leave the box, as if an infinite potential wall was located at the box boundary. The atomic continuum then reduces to an infinite *but discrete* set of stationary modes equally spaced by $\Delta p=\pi/r_{max}$ in momentum space, yielding the pseudocontinuum state density $d=r_{max}/\pi\sqrt{2E}$ on the energy scale. Within the box, eigenfunctions are obtained by diagonalizing H_0 in a basis of spherical Bessel functions $j_l(kr)$, which are free spherical waves of well defined angular momentum l spreading over all orientations of electronic momentum $\mathbf{k}$ [20,21]. In practice, the underlying basis consists of all the $j_l(kr)$ functions such that $j_l(kr_{max})=0$, thus fulfilling the simplest continuity condition with the outer region where all eigenfunctions vanish, and $0\leqslant k\leqslant k_{max}$ and $0\leqslant l\leqslant l_{max}$. The spherical Bessel functions exhibit the correct $\sin(kr-l\pi/2)/kr$ asymptotic r behavior: the basis suitably spans the whole $0\leqslant r\leqslant r_{max}$ range and is thus expected to provide a faithful representation of the ionization process.

III. DESCRIPTION OF IONIZATION

The STO basis that has been used in the present $\bar{p}+$H($1s$) calculations is defined by $l_{max}=5$ and the geometrical sequences of orbital exponents $\{\alpha_0,\beta,j_{max}\}$ listed in Table I. These parameters were chosen to give very accurate representations of the lower bound eigenstates and yield

TABLE I. Energy eigenvalues of the Hamiltonian (upper array) diagonalized in the even-tempered STO basis $\{l_{max}=5,\{\alpha_0,\beta,j_{max}\}_{l=0,\ldots,l_{max}}\}$ defined in the lower array.

l					
0	1	2	3	4	5
				5.430 75	4.415 09
		5.000 98	3.741 21	3.048 35	2.504 85
4.030 63	3.650 77	2.693 23	2.061 89	1.703 86	1.411 14
2.150 44	1.899 29	1.446 33	1.126 95	0.941 84	0.784 76
1.116 85	0.977 70	0.764 69	0.604 56	0.510 30	0.427 27
0.555 23	0.487 83	0.391 39	0.313 60	0.267 35	0.224 78
0.256 95	0.228 65	0.188 59	0.153 24	0.132 18	0.111 54
0.104 48	0.094 64	0.080 72	0.066 69	0.058 49	0.049 48
0.031 41	0.028 98	0.025 84	0.021 76	0.019 68	0.016 57
0.000 67	0.000 52	0.000 66	0.000 35	0.000 60	0.000 13
−0.007 73	−0.007 72	−0.007 65	−0.007 53	−0.007 26	−0.007 10
−0.010 17	−0.010 17	−0.010 17	−0.010 18	−0.010 20	−0.010 20
−0.013 88	−0.013 88	−0.013 88	−0.013 88	−0.013 88	−0.013 88
−0.020 00	−0.020 00	−0.020 00	−0.020 00	−0.020 00	
−0.031 25	−0.031 25	−0.031 25	−0.031 25		
−0.055 55	−0.055 55	−0.055 55			
−0.125 00	−0.125 00				
−0.500 00					

l	α_0	β	j_{max}
0	0.060	1.3	24
1	0.068	1.3	19
2	0.079	1.3	19
3	0.092	1.3	19
4	0.110	1.3	19
5	0.131	1.3	19

a dense discretization of the low-energy part of the continuum (see Table I). After diagonalizing H_0, all eigenstates with $E_n>6$ a.u. are removed from the diagonalized basis insomuch as they lie too high in the continuum to be significantly populated. Dynamical calculations are thus performed using the 295 eigenstates given in Table I (spherical harmonics are included up to $m=l$).

The main Bessel set that has been used is defined by $r_{max}=120$ a.u., $l_{max}=3$, and $k_{max}=2.5$ a.u.; all spherical harmonics are included up to $m=2$, yielding 856 states. H($1s$) and H($2p$) bound eigenstates are explicitly added to this basis before diagonalizing H_0 to speed up the convergence of the expansion with respect to the description of the lowestlying bound eigenstates. Table II contains the negative energy eigenvalues of the diagonalized Hamiltonian; the description of the excitation states can be regarded as exact from $n=1$ to 6. The radial box is not large enough to provide an accurate representation of the highest bound states that would extend beyond $r=120$ a.u.; the diagonalization procedure thus yields confined states that overlap the inner part of the true Rydberg states. The description of these highlying bound states can be bettered as desired by increasing r_{max}. Finally, the positive energy eigenvalues are not reported in Table II since a huge number of pseudocontinuum states are obtained up to $E_n\sim k_{max}^2/2$ (see Fig. 10 below).

A. Cross sections and probabilities

The partial cross sections for excitation into H($2s$) and H($2p$) states are displayed in Fig. 1 as a function of the impact energy E for 1 keV$\leqslant E\leqslant$1 MeV. The cross sections from both the present STO and Bessel calculations are in excellent agreement over the whole energy range. Fine agreement is also found with the monocentric results of Hall *et al.* [22], who employed a STO-like underlying basis with complex exponents [12], and with the calculations of Wells *et al.* [23], who solved the time-dependent Schrödinger equation (TDSE) on a three-dimensional spatial lattice grid. The cross sections obtained by means of two-center atomic calculations performed by Ermolaev [24] exhibit oscillatory structures; Toshima [25] has shown that these (artificial) oscillations are due to the momentum matching mechanism between bound and pseudocontinuum states belonging to different centers, and that they disappear for large enough bases.

Our ionization cross sections are presented in Fig. 2. Comparison was made in [1] with the experimental data of

TABLE II. Negative energy eigenvalues of the Hamiltonian diagonalized in the spherical Bessel basis $\{r_{max}=120$ a.u., $l_{max}=3$, and $k_{max}=2.5$ a.u.$\}$.

l			
0	1	2	3
−0.002 95	−0.003 09	−0.003 37	−0.003 76
−0.006 94	−0.007 00	−0.007 11	−0.007 26
−0.010 14	−0.010 15	−0.010 16	−0.010 18
−0.013 88	−0.013 88	−0.013 88	−0.013 88
−0.020 00	−0.020 00	−0.020 00	−0.020 00
−0.031 25	−0.031 25	−0.031 25	−0.031 25
−0.055 55	−0.055 55	−0.055 55	
−0.125 00	−0.125 00		
−0.500 00			

Knudsen *et al.* [26], the monocentric expansions of Hall *et al.* [22] and Schiwietz *et al.* [27], and the time-dependent Schrödinger equation, classical trajectory Monte Carlo and perturbative continuum distorted wave–eikonal initial state (CDW-EIS) results of Wells *et al.* [23] and Schultz *et al.* [28]. We add in Fig. 2 the results of Kirchner *et al.* [29] obtained by means of the basis generator method (BGM) [30]; they exhibit the same shape as the other close-coupling results, which all agree within 10%. We thus focus on a comparison of the results provided by the present STO and Bessel calculations.

First of all, we verified that high angular momenta are not necessary to obtain converged cross sections for ionization and $n=2$ excitation (Fig. 1) by increasing l_{max} from 3 to 5 within the Bessel expansion. The Bessel and STO results are in excellent agreement down to 5 keV; below this point, they start to deviate from each other and the STO cross section is

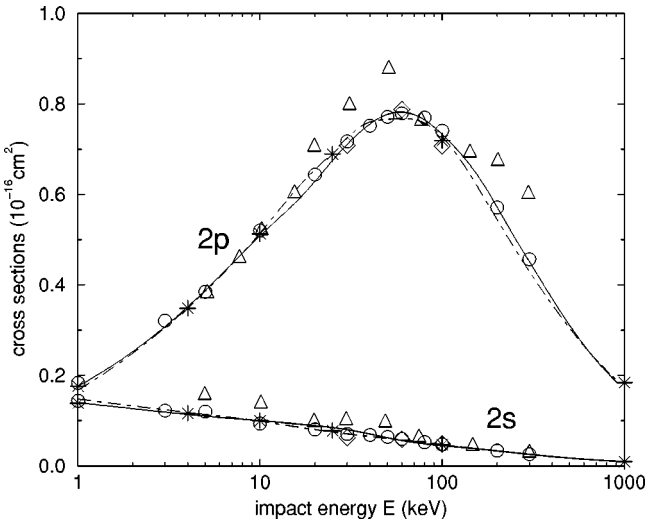

FIG. 1. $2s$ and $2p$ excitation cross sections for $\bar{p}+\mathrm{H}(1s)$ collisions: (——) $\{r_{max}=120$ a.u., $l_{max}=3$, and $k_{max}=2.5$ a.u.$\}$ Bessel expansion; $(*)$ $\{r_{max}=120$ a.u., $l_{max}=5$, and $k_{max}=2.5$ a.u.$\}$ Bessel expansion; (— – — –) STO expansion of Table I; (○) monocentric expansion of Hall *et al.* [22]; (△) two-center atomic results of Ermolaev [24]; (◇) TDSE results of Wells *et al.* [23].

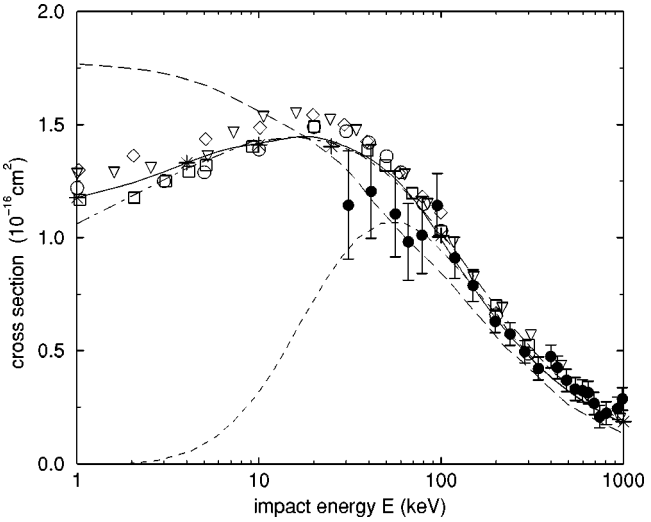

FIG. 2. Ionization cross sections for $\bar{p}+\mathrm{H}(1s)$ collisions: same symbols as in Fig. 1 and (□) monocentric expansion [27] of Schiwietz *et al.* (taken from [22]); (∇) BGM results of Kirchner *et al.* [29]; (— — —) CTMC, (– – –) CDW-EIS results of Wells *et al.* [23] and Schultz *et al.* [28]; (●) experimental data of Knudsen *et al.* [26].

finally ~10% smaller than the Bessel one at the lowest impact energy considered ($E=1$ keV). An anomalous population of the highest excitation states ($n>6$) appears in low-energy STO calculations, which breaks the expected decrease of Rydberg state population with n. Further, the disagreement with other monocentric predictions vanishes if this superfluous population is added to the ionization one. Although such a contamination can be justified by arguing that Rydberg states are analytic continuations of near-zero energy continuum wave functions, it rather shows the incompleteness of the STO expansion, which cannot produce diffuse enough pseudocontinuum states to compete with the high-lying bound states to absorb the remaining ionizing flux. Schiwietz *et al.* also pointed out convergence problems associated with the representation of eigenstates near the threshold, especially for the $\bar{p}$-H system [27]. Trapping of the ionization flux into diffuse bound states does not appear within the Bessel calculations, although they also include (approximate) high-lying Rydberg states, owing to the completeness of the underlying basis (see [31]).

In Fig. 3, we compare the weighted ionization probabilities $bP(b)$ obtained by means of the STO and Bessel expansions for $v=0.4$ a.u., $v=1$ a.u., and $v=3$ a.u. From low to high impact velocities, the weighted probabilites compare favorably so that the agreement of the corresponding cross sections is not fortuitous. The maximum contribution to the cross section is always found around $b=1.2$ a.u. The nuclear trajectories defined by $(v,b=1.2$ a.u.$)$ will therefore be considered as representative in the following illustrations of the ionization dynamics.

We present in Fig. 4 the temporal evolution of the $n=2$ excitation and ionization probabilities as a function of the scaled time $Z=vt$. Once again, the agreement between STO and Bessel calculations is good. Even if the excitation chan-

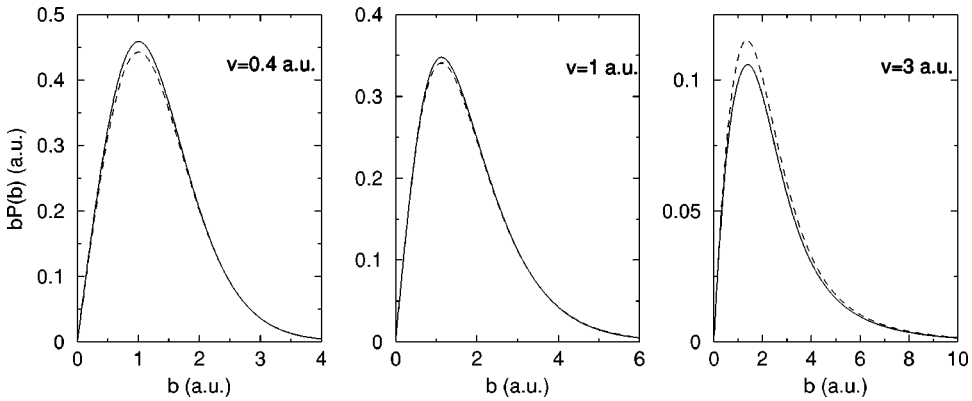

FIG. 3. Weighted probabilities $bP(b)$ for ionization in $\bar{p}+\mathrm{H}(1s)$ collisions as a function of the impact parameter b: (——) $\{r_{max}=120$ a.u., $l_{max}=3$, and $k_{max}=2.5$ a.u.$\}$ Bessel expansion; (– –) STO expansion of Table I.

nels are involved as intermediate states to promote the ionization flux up to the threshold at low velocities, it is noteworthy that the final ionization population is determined as early as $Z=10$ a.u.

Up to now, the STO expansion seems to be as adequate as the Bessel one to provide an accurate description of the ionization process. We now go deeper into this description, by studying the time evolution of spatial and momentum ionizing densities simultaneously.

B. Ejected electron distributions

1. STO versus Bessel expansions

Time samplings of the electron distributions obtained according to Eqs. (3) and (4) by means of the STO and Bessel expansions are presented in Figs. 5 and 6, respectively, for an intermediate impact velocity $v=1$ a.u. ($\equiv E=25$ keV) and the representative impact parameter $b=1.2$ a.u. All ionizing events occur quite suddenly from $Z=-5$ a.u to $Z=10$ a.u. (see Fig. 4). Within this range the spatial and momentum ionizing densities obtained by the STO and Bessel calculations are similar and depict the same ionization mechanism: a part of the electronic cloud, initially polarized along the internuclear axis, is compressed toward the target nucleus as the antiproton moves forward. The electronic energy consequently increases, giving rise to an unbound electron emitted with a velocity near the impact one. The whole ionizing cloud then rotates around the target, pushed away by the impinging antiproton but still subject to the fixed target nucleus field. Circular structures centered about the target appear in the STO spatial ionizing density around $Z=5$ a.u.; the Bessel expansion leads to a smoother density that expands further beyond the projectile location.

Major discrepancies between the STO and Bessel descriptions arise for $Z>5$ a.u. The STO expansion provides a spatial distribution that remains confined into an $r<10$ a.u. domain around the target. This picture cannot be considered as physical insomuch as an ionized electron is expected to escape from the target zone. Furthermore, the momentum distribution, whose shape is continuously changing as time elapses, exhibits sizable emission velocities so that **r** and **p** distributions cannot be related to each other. We conclude that *the STO expansion is unable to provide a coherent description of the evolution of the ionizing density in the outgoing part of the collision*; and, particularly, *it cannot represent the (expected) spread of the ionizing cloud.*

We now turn to the evolution of the ionizing density predicted by the Bessel expansion for $Z>5$ a.u. The total ionization probability reaches its asymptotic value $P^{ion}=0.285$ as early as $Z=10$ a.u. (see Fig. 4) and any further change in the electron distributions is due to PCI effects. From $Z=5$ to 20 a.u., two-center effects still influence the evolution of electron distributions; while expanding, most of the ionizing density proceeds on its way around the target. In this range, a sizable part of the cloud pulls ahead of the antiproton; the corresponding electrons mainly travel in the longitudinal direction with a transverse momentum near 0. The target nucleus no longer acts on this part of the ionizing cloud as time elapses further (from $Z=20$ to 40 a.u. in Fig. 6). The rotation of the cloud centered about the target is also ending

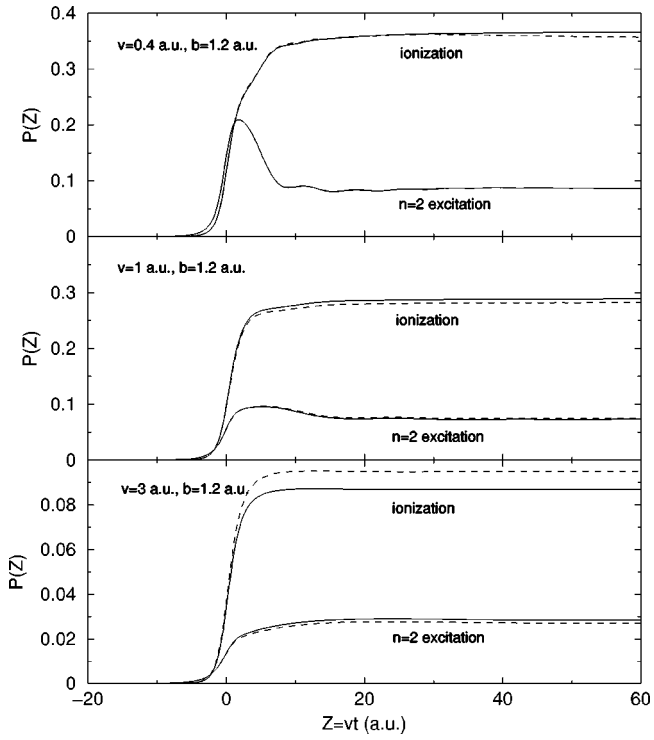

FIG. 4. Temporal evolution along representative nuclear trajectories (v,b) of $n=2$ excitation and ionization probabilities, as a function of the scaled time $Z=vt$: (——) $\{r_{max}=120$ a.u., $l_{max}=3$, and $k_{max}=2.5$ a.u.$\}$ Bessel expansion; (– –) STO expansion of Table I.

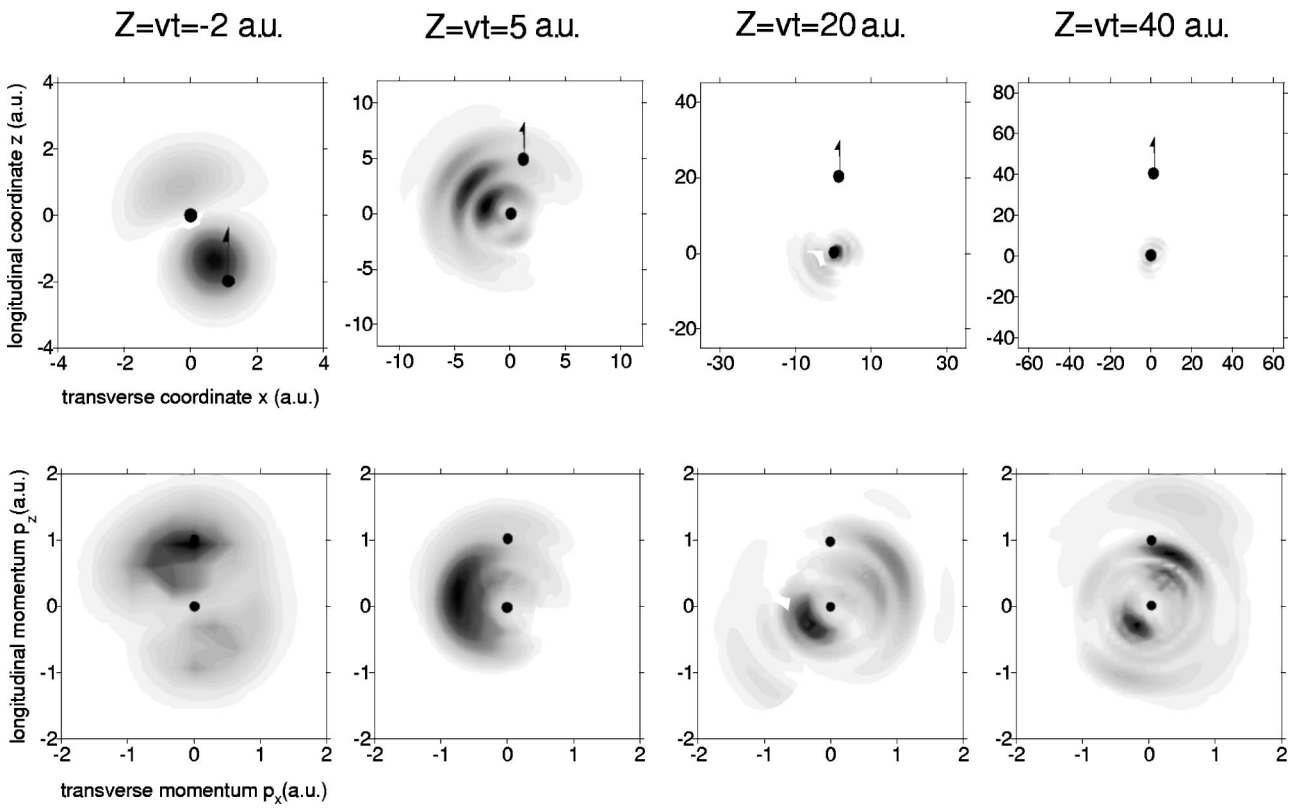

FIG. 5. Two-dimensional distributions of ejected electrons in coordinate and momentum spaces, as a function of the scaled time $Z=vt$, obtained by means of the STO expansion (Table I) for $\bar{p}+\mathrm{H}(1s)$ collisions; $v=1$ a.u. and $b=1.2$ a.u.. The black points indicate the nuclei positions.

because of the weakening of the $\bar{p}$-e^- interaction. This leads to a weak narrowing of the momentum space distribution around the target nucleus.

From low to intermediate impact velocities, the ionization process shares the same physical origin and most of the ionizing density is finally found in the left lower quadrant of both configuration and momentum spaces (see [1]). We now consider the case of high impact velocity in Fig. 7, which displays the time evolution of the ionizing distributions for $v=3$ a.u. and $b=1.2$ a.u. Ionization still occurs as a result of the compression of the electronic cloud toward the target nucleus (see $Z=-2$ a.u. in Fig. 7). Nevertheless, electrons are now emitted with a velocity smaller than the impact velocity and the projectile rapidly crosses the high-electronic-density area. The pull of the swift projectile on the ionizing cloud thus competes with the attractive p-e^- interaction only across the turning point, yielding a 90° rotation about the target nucleus. Furthermore, in the same Z interval new ionizing events appear, stemming from the pull of the fast projectile on the outer part of the electronic cloud: high impact velocities prevent the cloud from moving as a whole and outer electrons ($x>b$) are ionized in the positive transverse direction ($p_x>0$) according to the wake induced by the fast negatively charged projectile. This leads to a lobe-shaped structure for both configuration and momentum distributions, which tends to become more pronounced as the impact velocity increases.

Finally, the time evolution of the present quantum distributions strikingly reinforces the classical findings of Illescas and Riera, at least for negatively charged ion impact: whatever the impact velocity, all ionizing events occur within a small range $Z<10$ a.u. and PCI effects are weakly acting in the asymptotic region. Accordingly, the ionized electrons move quasifreely and their momentum **p** and position **r** are related by $\mathbf{r}=\mathbf{p}t$ to a good accuracy. This time scaling of the ejected electron distributions is clear in Figs. 6 and 7 for large Z. We further compare in Fig. 8 the one-dimensional momentum space distributions obtained for $v=3$ a.u., $b=1.2$ a.u., and $Z=50$ and 100 a.u. As stated in [1] for a lower impact velocity, all of the distributions remain identical within this Z interval, except that the longitudinal and transverse distributions are slightly shifted toward 0 because of the (above-mentioned) weakening of the $\bar{p}$-e^- interaction. These quasistationary momentum distributions, *which STO expansions do not succeed in representing* (see Fig. 5), emphasize that the main feature of the ionization mechanism is an early quasifree expansion of the ionizing cloud.

2. Reliability of the Bessel expansion

We now address the reliability of the Bessel description. Because of the lack of experimental data, we compare in Fig. 9 our results with the two center momentum space discretization (TCMSD) momentum distribution of Sidky and Lin [32] for $v=1$ a.u., $b=2.5$ a.u., and $Z=20$ a.u. The Bessel

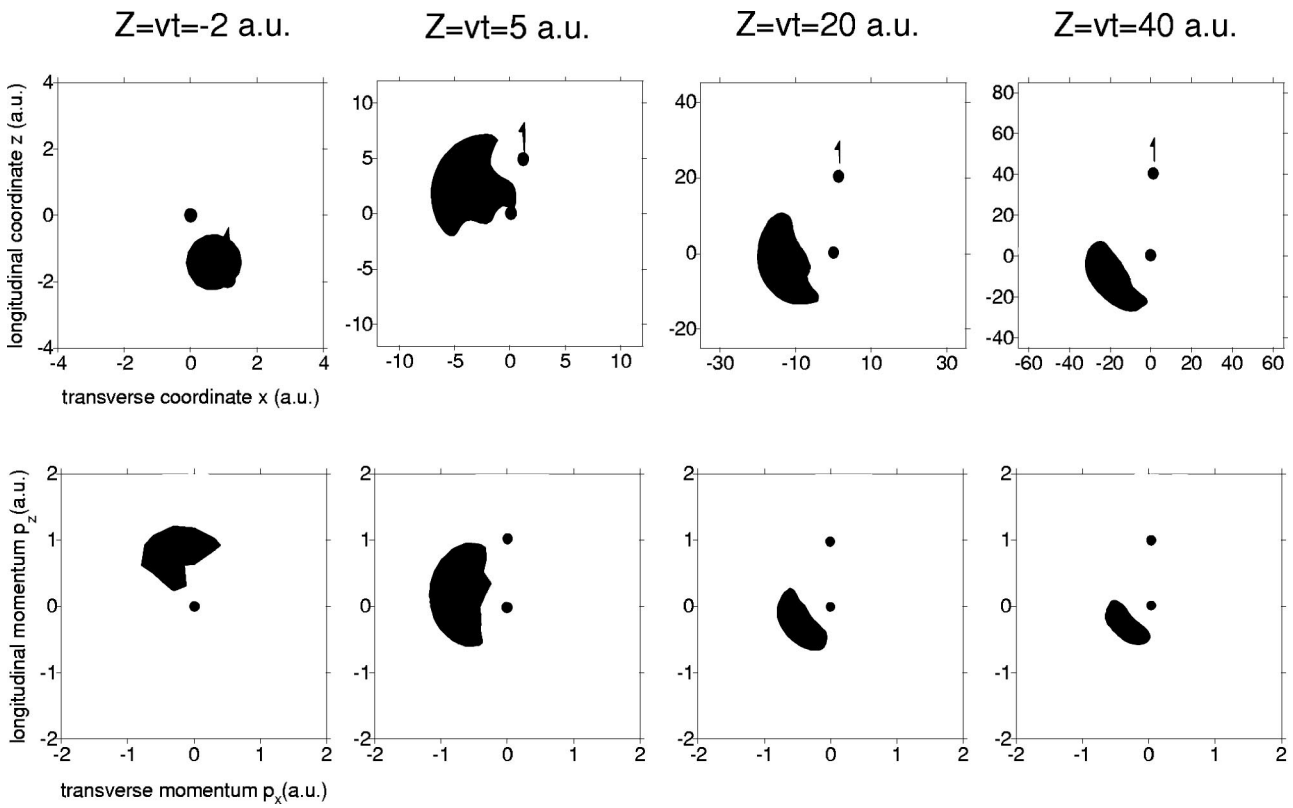

FIG. 6. Two-dimensional distributions of ejected electrons in coordinate and momentum spaces, as a function of the scaled time $Z=vt$, obtained by means of the $\{r_{max}=120$ a.u., $l_{max}=3$, and $k_{max}=2.5$ a.u.$\}$ Bessel expansion for $\bar{p}+\mathrm{H}(1s)$ collisions; $v=1$ a.u. and $b=1.2$ a.u. The black points indicate the nuclei positions.

and TCMSD distributions agree closely. The TCMSD and monocentric Bessel schemes differ in the underlying basis sets and numerical techniques used to solve the collisional problem; the agreement of the momentum distributions indicates that both calculations are converged and reliable. Moreover, the same agreement has been found for the other nuclear trajectories considered in [32]; the corresponding distributions are not presented for sake of conciseness. The ionizing densities presented in Figs. 6 and 7 are obtained from a Bessel expansion defined by $\{r_{max}=120$ a.u., $l_{max}=3$, $k_{max}=2.5$ a.u. $\}$. We also include in Fig. 9 the distribution resulting from a calculation in which l_{max} has been increased to 5 (yielding 1423 states). The momentum (and space) distributions do not significantly change, ensuring that the former calculation is converged with respect to l.

Both Bessel sets include spherical harmonics up to $m=2$ although $l_{max}>2$, to avoid cumbersome calculations. We checked that higher magnetic numbers marginally contribute to the description of the ionizing cloud in STO calculations and that the $m=2$ contribution within the Bessel calculations is already small. In the former case, the $m\geqslant 3$ contribution represents 0.16% of the total ionization probability and in the latter the $m=2$ contribution is 3.89%.

Controlling the adequacy of the parameters r_{max} and k_{max} is even simpler; it can be checked *a posteriori* that the momentum distribution vanishes for electronic momenta near k_{max} and that the extent of the configuration distribution does not exceed the r_{max} box. In practice, the size of the box sets an upper bound Z_m to the temporal range over which the evolution of the ionizing cloud can be accurately described. This limit corresponds to a spread of the ionizing cloud beyond the finite box. For $Z>Z_m$, unphysical ingoing waves appear in the configuration distribution as a result of flux reflexion on the bounding box wall. An absorbing (complex) potential, which acts at the box boundary, can be used to overcome this limitation; nevertheless, its use leads to a distortion of the high-p part of the momentum distribution that can be confounded with the physical narrowing of the distribution around zero, due to slowly acting PCI effects. So, rather than using an absorbing potential, it is therefore preferable to take r_{max} large enough to allow an accurate description of the ionizing cloud up to large (but finite) Z. Strictly speaking, asymptotic momentum distributions cannot be easily obtained unless r_{max} is huge. In practice, and according to the early quasifree expansion of the ionizing cloud, we define the asymptotic collisional region by $Z>Z_m$ with Z_m such that no major changes appear in the shape of momentum distributions for $Z>Z_m$.

From Fig. 9 and the above convergence checks, we conclude that *the monocentric Bessel expansion provides reliable distributions for ejected electrons in the outgoing part of the collision*.

3. Failures of STO expansions

We now aim at elucidating the properties of the STO expansion that allow an accurate prediction of ionization

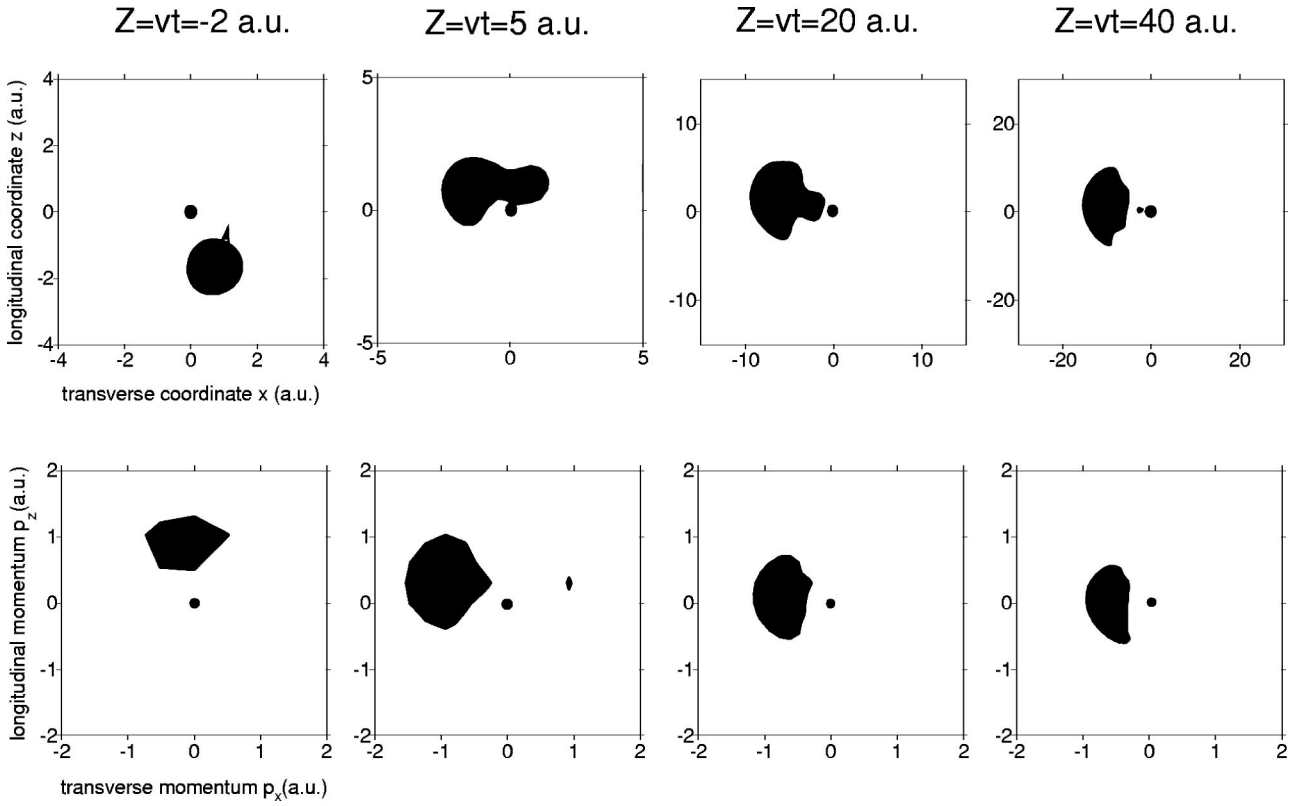

FIG. 7. Same as Fig. 6 for $v=3$ a.u. and $b=1.2$ a.u.

cross sections and probabilities but not a reliable description of the ionizing cloud for large Z.

The degree of approximation of the Bessel ionizing wave function by the STO expansion can be gauged from the overlap

$$S(v,b,Z)=\frac{|\langle\Psi^{ion}_{STO}|\Psi^{ion}_{Bessel}\rangle|}{N_{STO}N_{Bessel}}, \tag{6}$$

where $\Psi^{ion}_{STO}(v,b,Z,\mathbf{r})$ and $\Psi^{ion}_{Bessel}(v,b,Z,\mathbf{r})$ are the ionizing parts of the electronic wave functions obtained by the STO and Bessel calculations, respectively, and $N_{STO,Bessel}=\sqrt{\langle\Psi^{ion}_{STO,Bessel}|\Psi^{ion}_{STO,Bessel}\rangle}$ are normalization factors. The closer S is to unity, the more adequate the STO expansion to represent the ($l_{max}=3$) Bessel ionizing cloud, which is taken herein as the reference. The S values obtained along the nuclear trajectory ($v=1$ a.u., $b=1.2$ a.u.) are reported in Table III, yielding a quantitative counterpart to the comparison of Figs. 5 and 6. The STO expansion is sufficiently complete to represent the ionizing flux for $Z<5$ a.u. where $S>0.8$. Later on, the description worsens and $S\to 0$. It can be seen in Fig. 6 that $Z=5$ a.u. corresponds to a spread of the ionizing cloud beyond the $r\sim 10$ a.u. range around the target. As Ψ^{ion}_{STO} is expanded in terms of pseudocontinuum states Φ_{Elm} built according to Eq. (6), we present in Fig. 10 the radial part of one of these states, with $l=1$ and $E=0.488$ a.u. Also drawn is the radial part of the corresponding exact continuum state, arbitrarily normalized so that its first maximum matches that of the approximate state. The pseudocontinuum state closely represents the inner part of the exact continuum state for $r<10$ a.u. while the outer, asymptotic part is not correctly reproduced. This failure is related to the exponen-

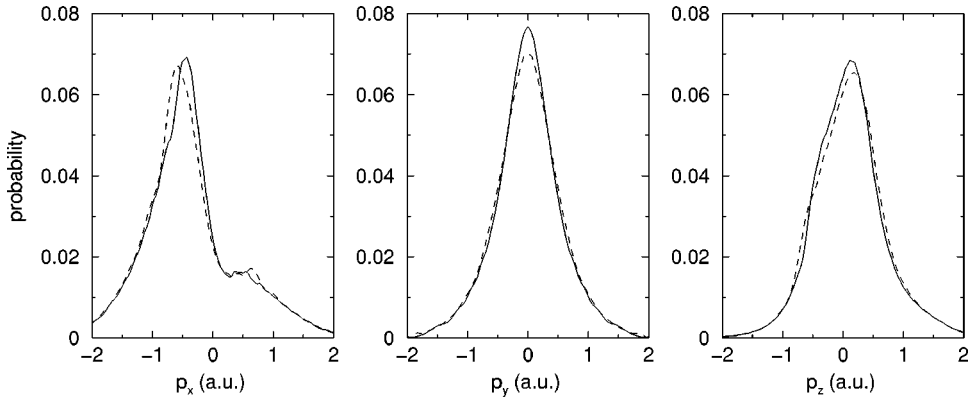

FIG. 8. One-dimensional momemtum distributions of ejected electrons, obtained by means of the $\{r_{max}=120$ a.u., $l_{max}=3$, and $k_{max}=2.5$ a.u.$\}$ Bessel expansion, for $\bar{p}+\mathrm{H}(1s)$ collisions; $v=3$ a.u., $b=1.2$ a.u., $Z=50$ a.u. (- - -) and $Z=100$ a.u. (——). p_x and p_z are the transverse and longitudinal momenta, p_y perpendicular to the collision plane.

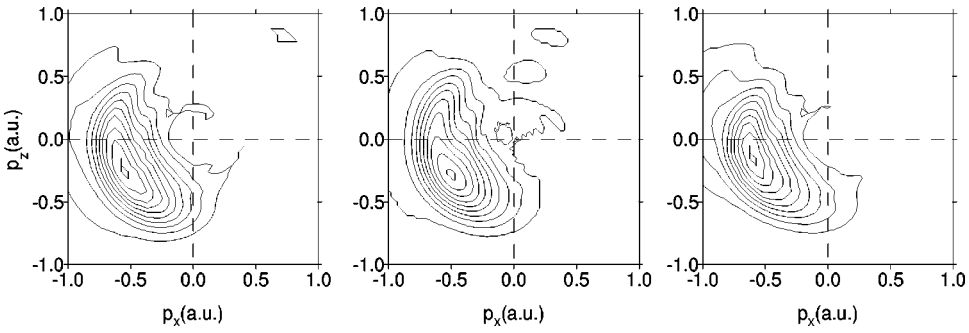

FIG. 9. Two-dimensional distributions of ejected electrons in momentum space for $\bar{p}+\mathrm{H}(1s)$ collisions; $v=1$ a.u., $b=2.5$ a.u., and $Z=20$ a.u.: (left) $\{r_{max}=120$ a.u., $l_{max}=3$, and $k_{max}=2.5$ a.u.$\}$ Bessel expansion; (middle) TC-MSD distribution of Sidky and Lin [32]; (right) $\{r_{max}=120$ a.u., $l_{max}=5$, and $k_{max}=2.5$ a.u.$\}$ Bessel expansion.

tially decaying r behavior of the STO basis functions, as stated 30 years ago by Hazi and Taylor [33]. Gaussian, hydrogenic, and Sturmian orbitals share the same drawback and are not expected to fare better in the description of exact continuum states. The usual expansions are therefore adequate for an accurate description of the ionizing flux over an $r\sim 10$ a.u. range around the target. Inelastic transitions from the entry channel to the continuum are suitably described within this range (see Fig. 4 from $Z=-2$ to 5 a.u.), yielding reliable probabilities and cross sections. The description worsens beyond this limited r range, leading to unphysical ejected electron distributions in the outgoing part of the collision: the cloud expansion cannot be represented by the STO development and the corresponding density is unphysically trapped around the target for large Z.

One can question whether this conclusion holds when a larger basis, including more diffuse orbitals, is employed. We thus consider a STO basis defined by $\{\alpha_0=0.001,\beta=1.3,j_{max}=40\}$ for $0\leqslant l\leqslant 5$ and $m\leqslant l$. It results in 861 orbitals which cover a wider spatial range than those of Table I. Dynamical calculations based on this expansion have not been performed; its ability to reproduce the Bessel ionizing wave function can be gauged *a priori* from the overlap,

$$S'(v,b,Z)=\frac{1}{N_{Bessel}^2}\sum_{E>0,lm}\left|\langle\phi_{Elm}|\Psi_{Bessel}^{ion}\rangle\right|^2, \qquad (7)$$

where Ψ_{Bessel}^{ion} and N_{Bessel} are defined as in Eq. (6), and ϕ_{Elm} are the pseudostates resulting from the diagonalization of H_0 in the enlarged basis. The S' values obtained using both STO expansions are reported in Table III for $v=1$ a.u. and $b=1.2$ a.u. It can be checked that $S'\equiv S$ (within numerical deviations) when the same STO expansion is employed. Further, the enlargement of the STO basis does not significantly improve the description of the ionizing cloud. The addition of diffuse orbitals to the basis yields higher-lying Rydberg states through diagonalization but the density and accuracy of the pseudostates remain as poor as before. The second STO basis is large enough to certify that expansions in terms of *any* exponentially decaying basis functions are unable to provide a reliable description of the ionizing flux in the outgoing part of the collision.

The basis of spherical Bessel functions is much better conditioned with respect to the representation of the atomic continuum. The key points of this expansion are (i) the confinement of the collisional problem into a finite box and (ii) the use of a complete basis within this box. Point (i) leads to a discretization of the atomic continuum with a corresponding state density $d=r_{max}/\pi\sqrt{2E}$ on the energy scale. The $\{j_l(kr)\}$ basis is strictly complete in the limit $l_{max},k_{max}\rightarrow\infty$; in practice, huge values of electronic momenta are not expected to contribute to the description of the ionizing cloud and the basis is restricted to $l\leqslant l_{max}$ and $k\leqslant k_{max}$. It can be checked whether the retained basis fulfills point (ii) by comparing the density of pseudocontinuum states obtained after diagonalization of H_0 with the expected one, d. A representative comparison is made in Fig. 10 for the $l=1$ symmetry. Small deviations from the expected behavior are found for $E<1$ a.u., due to the contribution of low-k $j_l(kr)$ functions to the description of bound eigenstates. Finally, we illustrate in Fig. 10 the ability of the Bessel expansion to yield pseudocontinuum states that perfectly fit the exact ones within the box. The reliable description of the evolution of the ionizing cloud relies on this accurate representation of the atomic spectrum.

IV. SUMMARY

We performed a thorough study of the ability of close-coupling expansions to describe ionization in $\bar{p}+\mathrm{H}(1s)$ collisions. Monocentric expansions in terms of even-tempered Slater-type orbitals were first considered. They provide a coarse description of the atomic continuum, which consists of a few pseudostates that closely represent the inner part of the exact continuum states but rapidly vanish for $r>10$ a.u., because of the exponentially decaying r behavior of the basis functions. Therefore the STO expansion can fairly describe the ionization flux over an $r\sim 10$ a.u. range around the target.

TABLE III. Overlaps $S(v,b,Z)$ and $S'(v,b,Z)$ [see Eqs. (6) and (7)] as a criterion of the ability of STO basis to reproduce the Bessel ionizing wave function, for $\bar{p}+\mathrm{H}(1s)$ collisions and nuclear trajectory ($v=1$ a.u., $b=1.2$ a.u.). The subscripts STO1 and STO2 refer to the basis defined in Table I and $\{\alpha_0=0.001,\beta=1.3,j_{max}=40\}_{l=0,\ldots,5}$, respectively.

Z (a.u.)	S_{STO1}	S'_{STO1}	S'_{STO2}
−2	0.984	0.993	0.996
1	0.987	0.992	0.996
5	0.798	0.787	0.813
10	0.503	0.504	0.537
20	0.276	0.288	0.303
40	0.127	0.127	0.145

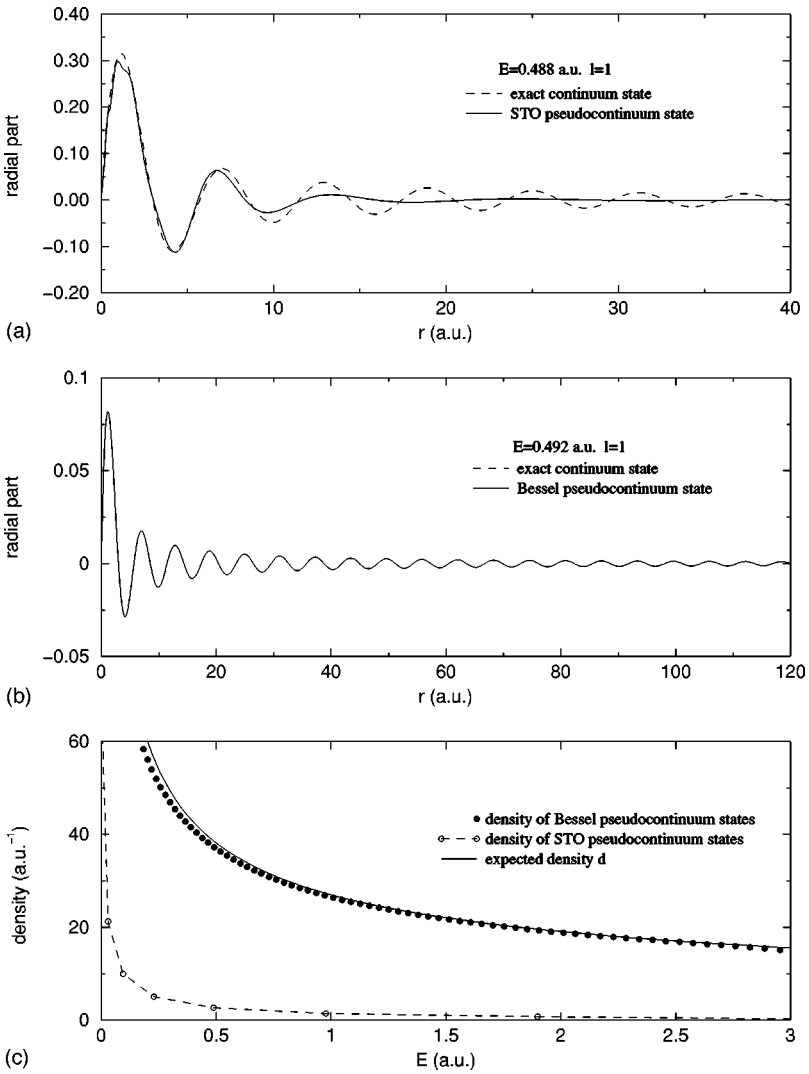

FIG. 10. Ability of the spherical Bessel and STO underlying basis to yield an accurate description of the atomic continuum through diagonalization of the Hamiltonian. (a),(b) Comparison of the radial part of the exact and approximate continuum states of energy E and angular momentum l (the Bessel pseudocontinuum state cannot be distinguished from the exact one); (c) density of pseudocontinuum states, compared with the expected density $d=r_{max}/\pi\sqrt{2E}$ (see Sec. II B), as a function of the atomic energy E.

Inelastic transitions from the entry channel to the continuum are suitably and entirely described within this range, yielding reliable probabilities and total cross sections. The description worsens as the ionizing cloud tends to expand beyond the limited r range, leading to unphysical ejected electron distributions in the outoing part of the collision.

A set of Gaussian, (scaled) hydrogenic, or Sturmian orbitals can be used as an alternative to the STO one. All these functions exponentially decay with r, lead to equivalent descriptions of the continuum for large expansions, and are not expected to fare better than STOs in the representation of the ionizing cloud. Multicentered treatments, in which similar underlying bases belong to different centers (target and projectile [8,13–15] and/or third center [16,17,34]), surely improve the description of the ionizing flux up to larger internuclear distances. Nevertheless, all subsets have a short range around their corresponding centers that impedes a faithful description of the spreading ionizing cloud in the asymptotic region. The ionizing density now remains trapped about the various centers considered in the calculation. The usual interpretation of asymptotic probabilities in terms of direct (target-centered), saddle-point (mid-centered), and ECC (projectile-centered) contributions to ionization is thus physically doubtful, notwithstanding the fact that the total ionization probability is reliable.

We reviewed the construction of the spherical Bessel expansion, whose success in providing reliable ejected electron distributions relies on a careful discretization of the atomic continuum, in terms of spherical Bessel functions confined in a finite box. We ascertained the reliability of the method and enlarged our previous study of ionizing $\bar{p}+\mathrm{H}(1s)$ collisions from low to high impact velocities. In slow collisions, electrons are emitted around $Z=0$ in the longitudinal direction with a velocity near the impact one; two-center effects then induce a rotary motion of the ionizing cloud around the target, which rapidly ends up in the left lower quadrant of both configuration and momentum spaces. In fast collisions, the electrons are initially emitted with a velocity smaller than the impact one; the two nuclei thus compete over a smaller temporal range, and the rotation ends up in the negative transverse direction ($p_z\sim 0, p_x<0$); further, outer electrons ($x>b$) are ejected in the positive transverse direction ($p_z\sim 0, p_x>0$) according to the wake induced by the swift projectile, yielding a lobe-shaped structure for the ionizing distributions. Whatever the impact velocity, we verified that

two-center effects influence the ionization dynamics only over a small range of internuclear distances. Later on, PCI effects are weakly acting and the main feature of the ionization process is a quasiuniform expansion of the cloud.

ACKNOWLEDGMENT

The author acknowledges Dr. Emil Y. Sidky for providing him with the TCMSD data of Fig. 9.

[1] B. Pons, Phys. Rev. Lett. **84**, 4569 (2000).
[2] J. Ullrich, R. Moshammer, R. Dorner, O. Jagutski, V. Mergel, H. Schmidt-Bocking, and L. Spielberger, J. Phys. B **30**, 2917 (1997).
[3] R. Moshammer, J. Ullrich, M. Unverzagt, W. Schmidt, P. Jardin, R. E. Olson, R. Mann, R. Dorner, V. Mergel, U. Buck, and H. Schmidt-Bocking, Phys. Rev. Lett. **73**, 3371 (1994).
[4] M. E. Rudd, Y.-K. Kim, D. H. Madison, and T. J. Gay, Rev. Mod. Phys. **64**, 441 (1992).
[5] G. W. Kerby III, M. W. Gealy, Y.-Y. Hsu, M. E. Rudd, D. R. Schultz, and C. O. Reinhold, Phys. Rev. A **51**, 2256 (1995).
[6] Clara Illescas and A. Riera, Phys. Rev. Lett. **80**, 3029 (1998).
[7] N. Stoltherfoht, R. D. DuBois and R. D. Rivarola, *Electron Emission in Heavy Ion-Atom Collisions* (Springer, Berlin, 1997).
[8] N. Toshima, Phys. Rev. A **50**, 3940 (1994); **59**, 1981 (1999).
[9] G. B. Crooks and M. E. Rudd, Phys. Rev. Lett. **25**, 1599 (1970).
[10] R. E. Olson, Phys. Rev. A **27**, 1871 (1983).
[11] R. Shakeshaft, Phys. Rev. A **18**, 1930 (1978).
[12] A. L. Ford, E. Fitchard, and J. F. Reading, Phys. Rev. A **16**, 133 (1977).
[13] W. Fritsch and C. D. Lin, J. Phys. B **15**, 1255 (1982).
[14] T. G. Winter, Phys. Rev. A **33**, 3842 (1986).
[15] J. Kuang and C. D. Lin, J. Phys. B **30**, 101 (1997).
[16] T. G. Winter and C. D. Lin, Phys. Rev. A **29**, 3071 (1984).
[17] B. M. McLaughin, T. G. Winter, and J. F. McCann, J. Phys. B **30**, 1043 (1997).
[18] C. Harel, H. Jouin, B. Pons, L. F. Errea, L. Mendez, and A. Riera, Phys. Rev. A **55**, 287 (1997).
[19] W. H. Press, S. A. Teukolsky, W. T. Vetterling, and B. P. Flannery, *Numerical Recipes* (Cambridge University Press, Cambridge, 1992).
[20] C. Cohen-Tannoudji, B. Dui, and F. Laloe, *Mécanique Quantique* (Hermann, Paris, 1977).
[21] *Handbook of Mathematical Functions*, edited by M. Abramowitz and I. A. Stegun (Dover, New York, 1970).
[22] K. A. Hall, J. F. Reading, and A. L. Ford, J. Phys. B **29**, 6123 (1996).
[23] J. C. Wells, D. R. Schultz, P. Gavras, and M. S. Pindzola, Phys. Rev. A **54**, 593 (1996).
[24] A. M. Ermolaev, in *Atomic Physics with Positrons*, Vol. 169 of *NATO Advaced Study Istitute, Series B: Physics*, edited by J. W. Humberston and E. A. G. Armour (Plenum, New York, 1987).
[25] N. Toshima, J. Phys. B **30**, L131 (1997).
[26] H. Knudsen, U. Mikkelsen, K. Paludan, K. Kirsebom, S. P. Moller, E. Uggerhoj, J. Slevin, M. Charlton, and E. Morenzoni, Phys. Rev. Lett. **74**, 4627 (1995).
[27] G. Schiwietz, U. Wille, R. Diez Muino, P. D. Fainstein, and P. L. Grande, J. Phys. B **29**, 307 (1996).
[28] D. R. Schultz, P. S. Krstic, C. O. Reinhold, and J. C. Wells, Phys. Rev. Lett. **76**, 2882 (1996).
[29] T. Kirchner, H. J. Ludde, O. J. Kroneisen, and R. M. Dreizler, Nucl. Instrum. Methods Phys. Res. B **154**, 46 (1999).
[30] O. J. Kroneisen, H. J. Ludde, T. Kirchner, and R. M. Dreizler, J. Phys. A **32**, 2141 (1999).
[31] A. Riera, Comments At. Mol. Phys. **1**, 131 (2000).
[32] Emil Y. Sidky and C. D. Lin, J. Phys. B **31**, 2949 (1998).
[33] A. U. Hazi and H. S. Taylor, Phys. Rev. A **1**, 1109 (1970).
[34] L. F. Errea, C. Harel, C. Illescas, H. Jouin, L. Mendez, B. Pons, and A. Riera, J. Phys. B **31**, 3199 (1998).